Physics Letters B 731 (2014) 126–130

Contents lists available at ScienceDirect

Physics Letters B

www.elsevier.com/locate/physletb

Fluid dynamics with saturated minijet initial conditions in ultrarelativistic heavy-ion collisions

R. Paatelainen [a,b], K.J. Eskola [a,b], H. Niemi [a,b,*], K. Tuominen [c,b]

[a] Department of Physics, PO Box 35, FI-40014 University of Jyväskylä, Finland
[b] Helsinki Institute of Physics, PO Box 64, FI-00014 University of Helsinki, Finland
[c] Department of Physics, PO Box 64, FI-00014 University of Helsinki, Finland

ARTICLE INFO

Article history:
Received 29 October 2013
Received in revised form 31 January 2014
Accepted 10 February 2014
Available online 14 February 2014
Editor: J.-P. Blaizot

ABSTRACT

Using next-to-leading order perturbative QCD and a conjecture of saturation to suppress the production of low-energy partons, we calculate the initial energy densities and formation times for the dissipative fluid dynamical evolution of the quark–gluon plasma produced in ultrarelativistic heavy-ion collisions. We identify the model uncertainties and demonstrate the predictive power of the approach by a good global agreement with the measured centrality dependence of charged particle multiplicities, transverse momentum spectra and elliptic flow simultaneously for the Pb+Pb collisions at the LHC and Au+Au at RHIC. In particular, the shear viscosity in the different phases of QCD matter is constrained in this new model simultaneously by all these data.

The main goal of ultrarelativistic heavy-ion collisions at the Large Hadron Collider (LHC) and the Relativistic Heavy-Ion Collider (RHIC) is to determine the thermodynamic and kinetic properties of strongly interacting matter. The measured hadronic transverse momentum (p_T) spectra at the LHC and RHIC provide convincing evidence for a formation of a strongly collective system and a nearly thermalized quark–gluon plasma (QGP) [1]. In particular, the observed systematics of the Fourier harmonics $v_n = \langle \cos(n\phi) \rangle$ of the azimuth-angle distributions, are remarkably consistent with a low-viscosity QCD matter whose expansion and cooling are describable with dissipative relativistic fluid dynamics [2–12].

The essential inputs to the fluid dynamics are the initial energy density and flow of the matter created in the collision. However, the final state observables like multiplicities, p_T spectra and v_n, are also strongly affected through the fluid dynamical expansion by the viscosity and the equation of state (EoS). Thus the entire space-time evolution, including partons in the colliding nuclei, the primary production and thermalization of QCD matter and the subsequent fluid dynamical evolution, becomes highly convoluted. Description of all these dynamics in a coherent way, leading to quantitative predictions and a meaningful determination of the QCD matter properties from the measurements, provides an ultimate challenge in the field. As discussed in this Letter, the determination of, e.g., the temperature dependence of the shear viscosity-to-entropy ratio $\eta/s(T)$ calls for a simultaneous theory analysis of all possible bulk (low-p_T) observables at the LHC and RHIC.

Parton saturation is a viable mechanism to control the otherwise unsuppressed production of soft small-p_T quanta in hadronic and nuclear collisions [13–16]. In essence saturation means that there exists a semihard scale controlling the particle production in the collision. In the perturbative QCD (pQCD) + saturation model we consider here, the primary particle production in A+A collisions is computed in collinear factorization by approaching the saturation at semi-hard scales from the perturbatively controllable high-p_T side [17,18]. Perturbative QCD provides an excellent description of hard processes in hadronic and nuclear collisions at interaction scales $Q \gtrsim 1$ GeV [19]. Moreover, this model allows for a quantification of the particle production uncertainties, and their propagation through the fluid dynamical evolution in nuclear collisions [18]. In addition to the internal consistency of the pQCD-based approach, it should be noted that perturbative primary gluon production in heavy-ion collisions is complementary to the Color-Glass Condensate models [20] which build on soft gluon fields. If these different high-energy QCD approaches produce similarly successful heavy-ion phenomenology, the overall uncertainty in determining the QCD matter properties can be dramatically reduced.

The present work has roots in the so-called EKRT saturation model [17], which successfully predicted the multiplicities and p_T spectra in central A+A collisions at RHIC and LHC [21–24], and also the centrality dependence at RHIC [25] (cf. Fig. 23(a) in [26]). Here we use the next-to-leading-order (NLO)-improved pQCD + saturation model of [18] to calculate the initial QGP energy density profiles and formation times, and combine these with viscous fluid

* Corresponding author.

http://dx.doi.org/10.1016/j.physletb.2014.02.018

dynamics. We analyze the centrality dependence of charged particle multiplicities, p_T spectra and elliptic flow (v_2) at the LHC and RHIC in terms of the few physical key-parameters of the model. We show that a good simultaneous description of all these observables can indeed be obtained without retuning the model from one collision system (cms-energy, nuclei, centrality) to another. This results in the robust predictive power of the approach, originating from the pQCD calculation of the QGP initial conditions. Most importantly, this predictive power enables us to study and restrict the ratio $\eta/s(T)$ in the different QCD-matter phases more consistently in a simultaneous multiobservable analysis of the LHC and RHIC data.

Let us then discuss the details of our model [18]. The rigorously calculable part is the minijet E_T production in an A+A collision, in a rapidity interval Δy and above a p_T scale p_0,

$$\frac{\mathrm{d}E_T}{\mathrm{d}^2\mathbf{s}} = T_A\left(\mathbf{s}+\frac{\mathbf{b}}{2}\right)T_A\left(\mathbf{s}-\frac{\mathbf{b}}{2}\right)\sigma\langle E_T\rangle_{p_0,\Delta y,\beta}, \tag{1}$$

where $\mathbf{s}=(x,y)$ is the transverse location, $\mathbf{b}$ the impact parameter, and $T_A(\mathbf{s})$ the standard nuclear thickness function with the Woods–Saxon nuclear density profile. The first E_T-moment of the minijet E_T distribution, $\sigma\langle E_T\rangle_{p_0,\Delta y,\beta}$ [18,27] is in NLO

$$\sigma\langle E_T\rangle_{p_0,\Delta y,\beta} = \sum_{n=2}^{3}\frac{1}{n!}\int[\mathrm{DPS}]_n\frac{\mathrm{d}\sigma^{2\to n}}{[\mathrm{DPS}]_n}\tilde{S}_n, \tag{2}$$

where $\mathrm{d}\sigma^{2\to n}$ are the collinearly factorized minijet production cross sections and $[\mathrm{DPS}]_n$ denote the phase–space differentials for the $2\to 2$ and $2\to 3$ cases [18,28]. We apply the CTEQ6M parton distribution functions (PDFs) [29] with the EPS09s impact-parameter dependent nuclear PDFs [30]. The measurement functions $\tilde{S}_2$ and $\tilde{S}_3$ define the hard scattering in terms of the minijet transverse momenta $p_{T,i}$ and the cut-off scale p_0, as well as the total minijet E_T produced in Δy:

$$\tilde{S}_n = \Theta\left(\sum_{i=1}^{n}p_{T,i}\geqslant 2p_0\right)E_{T,n}\Theta(E_{T,n}\geqslant\beta p_0), \tag{3}$$

where $E_{T,n}=\sum_{i=1}^{n}\Theta(y_i\in\Delta y)p_{T,i}$ and Θ is the step function. These functions, analogous to the jet definitions [31], are constructed so that $\sigma\langle E_T\rangle_{p_0,\Delta y,\beta}$ is a well-defined, infrared- and collinear-safe, quantity to compute. The hardness-parameter β defines the minimum E_T in the interval Δy. As discussed in [18], any $\beta\in[0,1]$ is acceptable for the rigorous NLO computation.

Following the new angle in formulating the minijet saturation [18], the E_T production is expected to cease when the $3\to 2$ and higher-order partonic processes start to dominate over the conventional $2\to 2$ processes. For a central collision of identical nuclei of radii R_A this leads to a transversally averaged saturation criterion $E_T(p_0,\sqrt{s_{NN}},\Delta y,\beta)=K_{\mathrm{sat}}R_A^2p_0^3\Delta y$, with an unknown, α_s-independent, proportionality constant $K_{\mathrm{sat}}\sim 1$. Generalizing to non-zero impact parameters and localizing in the transverse coordinate plane gives

$$\frac{\mathrm{d}E_T}{\mathrm{d}^2\mathbf{s}}\left(p_0,\sqrt{s_{NN}},\Delta y,\mathbf{s},\mathbf{b},\beta\right)=\frac{K_{\mathrm{sat}}}{\pi}p_0^3\Delta y, \tag{4}$$

where the l.h.s. is the p_0-dependent NLO pQCD calculation defined in Eq. (1).

For given K_{sat} and β, we solve the above equation for $p_0=p_{\mathrm{sat}}(\sqrt{s_{NN}},A,\mathbf{s},\mathbf{b};K_{\mathrm{sat}},\beta)$, and obtain the total $\mathrm{d}E_T/\mathrm{d}^2\mathbf{s}$ in a mid-rapidity unit $\Delta y=1$ at saturation from the r.h.s. as $K_{\mathrm{sat}}p_{\mathrm{sat}}^3/\pi$. Once the solution p_{sat} is known, the local energy density is obtained [21,23] as

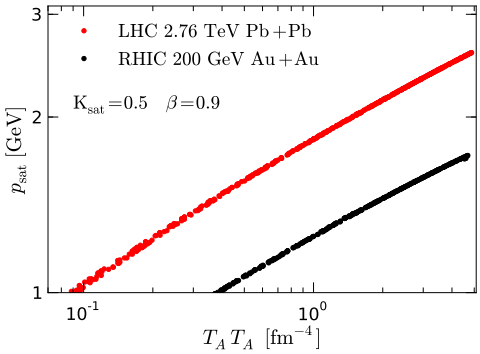

Fig. 1. (Color online.) Examples of the saturation momenta obtained for the LHC and RHIC A+A collisions, as functions of T_AT_A. See text for details.

$$\varepsilon(\mathbf{s},\tau_s=1/p_{\mathrm{sat}})=\frac{\mathrm{d}E_T}{\mathrm{d}^2\mathbf{s}\,\tau_s\Delta y}=\frac{K_{\mathrm{sat}}}{\pi}p_{\mathrm{sat}}^4, \tag{5}$$

where the local formation time is $\tau_s=1/p_{\mathrm{sat}}$.

Fig. 1 shows examples of $p_{\mathrm{sat}}(\sqrt{s_{NN}},A,\mathbf{s},\mathbf{b};K_{\mathrm{sat}},\beta)$ as a function of T_AT_A, calculated for fixed values of K_{sat},β and with $b=0$ and three other fixed impact parameters corresponding to the centrality classes 0–5%, 20–30% and 40–50% in $\sqrt{s_{NN}}=2.76$ TeV Pb+Pb collisions at the LHC and 200 GeV Au+Au at RHIC. To a very good approximation, the $\mathbf{b}$ and $\mathbf{s}$ dependence of p_{sat} comes only through T_AT_A. This is due to the weak $\mathbf{s}$ dependence of the nPDFs near the centres of the nuclei [30]. The approximate power-law scaling behavior seen at large T_AT_A can then be understood as explained in [32].

We identify two main uncertainties in mapping the pQCD + saturation calculation to an initial state for fluid dynamics: (i) The energy density given by Eq. (5) is at a time $\tau_s=1/p_{\mathrm{sat}}$, i.e. different at each transverse point $\mathbf{s}$, while for fluid dynamics we need the initial condition at a fixed time τ_0. (ii) We cannot trust the pQCD calculation down to $p_{\mathrm{sat}}\to 0$, but we need to set a minimum scale $p_{\mathrm{sat}}^{\mathrm{min}}\gg\Lambda_{\mathrm{QCD}}$. Wherever $p_{\mathrm{sat}}\geqslant p_{\mathrm{sat}}^{\mathrm{min}}$ we can use the pQCD calculation, but the other regions, i.e. low density edges, need to be treated separately.

We fix a minimum saturation scale as $p_{\mathrm{sat}}^{\mathrm{min}}=1$ GeV. Correspondingly, the maximum formation time in our model is $\tau_0=1/p_{\mathrm{sat}}^{\mathrm{min}}$. Then, we evaluate the energy densities from $\tau_s(\mathbf{s})$ to τ_0 using either the Bjorken free streaming $\varepsilon(\tau_0)=\varepsilon(\tau_s)(\tau_s/\tau_0)$ (FS) or the Bjorken hydrodynamic scaling solution $\varepsilon(\tau_0)=\varepsilon(\tau_s)(\tau_s/\tau_0)^{(4/3)}$ (BJ). We take these two limits to represent the uncertainty in the early pre-thermalization evolution: In the free streaming case the transverse energy is preserved, while the other limit corresponds to the case where a maximum amount of the transverse energy is reduced by the longitudinal pressure.

To obtain the energy density $\varepsilon(\mathbf{s},\tau_0)$ in the transverse region where $p_{\mathrm{sat}}<p_{\mathrm{sat}}^{\mathrm{min}}$, we use an interpolation $\varepsilon=C(T_AT_A)^n$, where C is a constant and the power $n=\frac{1}{2}[(k+1)+(k-1)\tanh(\{\sigma_{NN}T_AT_A-g\}/\delta)]$ with the total inelastic nucleon–nucleon cross-section σ_{NN}, and $g=\delta=0.5$ fm^{-2}. This smoothly connects the FS/BJ-evolved pQCD energy density $\varepsilon(p_{\mathrm{sat}}^{\mathrm{min}})=C(T_AT_A)^k$ to the binary profile $\varepsilon\propto T_AT_A$ at the dilute edge. Full specification of the initial conditions for the fluid dynamics requires also the components of the shear-stress tensor and the fluid velocity. These are set initially to zero.

For the fluid-dynamical evolution, we use the state-of-the art 2+1 D setup previously employed in Ref. [11,12,33], assuming longitudinal boost invariance, a zero net-baryon density and thermalization at τ_0. The equations of motion are given by the conservation laws for energy and momentum, $\partial_\mu T^{\mu\nu}=0$. The evolution equation of the shear-stress tensor $\pi^{\mu\nu}=T^{\langle\mu\nu\rangle}$ is given by transient relativistic fluid dynamics [34–36],

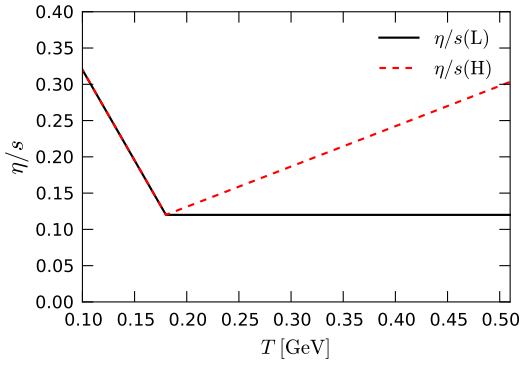

Fig. 2. (Color online.) Shear viscosity-to-entropy ratio as a function of temperature.

$$\tau_\pi \dot{\pi}^{\langle\mu\nu\rangle} + \pi^{\mu\nu} = 2\eta\sigma^{\mu\nu} - c_1\pi^{\mu\nu}\theta - \left(c_2\sigma^{\langle\mu}{}_\lambda - c_3\pi^{\langle\mu}{}_\lambda\right)\pi^{\nu\rangle\lambda},$$

where the co-moving time derivative $u^\mu\partial_\mu$ is denoted by the dot, η is the shear viscosity coefficient, $\sigma^{\mu\nu} = \partial^{\langle\mu}u^{\nu\rangle}$ is the shear tensor, $\theta = \partial_\mu u^\mu$ is the expansion rate, and the angular brackets $\langle\rangle$ denote the symmetrized and traceless projection, orthogonal to the fluid four-velocity u^μ. The coefficients of the non-linear terms are taken to be $c_1 = 4\tau_\pi/3$, $c_2 = 10\tau_\pi/7$ and $c_3 = 9/(70p)$, where p is the thermodynamic pressure and $\tau_\pi = 5\eta/(\varepsilon + p)$. For details of the numerical algorithm, see Refs. [11,37].

The hadron spectra are calculated with the Cooper–Frye freeze-out procedure [38] by using Israel's and Stewart's 14-moment ansatz for the dissipative correction to the local equilibrium distribution function, $\delta f_i = f_{0i}p_i^\mu p_i^\nu\pi_{\mu\nu}/[2T^2(\varepsilon + p)]$, where $f_{0i} = \{\exp[(u_\mu p_i^\mu - \mu_i)/T] \pm 1\}^{-1}$, with the index i indicating different hadron species and p_i^μ the 4-momentum of the corresponding hadron. The freeze-out temperature is here always $T_{\rm dec} = 100$ MeV. After calculating the thermal spectra, we include the contribution from all 2- and 3-particle decays of unstable resonances in the EoS.

We use the lattice QCD and hadron resonance gas (HRG) based EoS $s95p$-PCE-v1 [39] with a chemical freeze-out temperature $T_{\rm chem} = 175$ MeV. Although the rather high $T_{\rm chem}$ leads to an overabundance of protons, it however reproduces the low-$p_{\rm T}$ region of the $p_{\rm T}$-spectra much better than, e.g., $T_{\rm chem} = 150$ MeV.

For a rough but realistic (non-constant [40]) shear viscosity description, we assume the ratio η/s to decrease linearly as a function of temperature in the hadronic phase, be in a minimum at the matching-temperature 180 MeV of the HRG/QGP phases in the used EoS, and either to increase or stay constant vs. T in the QGP phase [11,12]. Fig. 2 shows the $\eta/s(T)$ which in our model best reproduce the v_2 coefficients simultaneously at RHIC and LHC.

At this point, we have a fixed model with four *correlated* unknowns, $\{K_{\rm sat}, \beta, {\rm BJ/FS}, \eta/s(T)\}$, to be determined using the LHC and RHIC data on the centrality dependence of the charged particle multiplicities, p_T spectra and v_2. We proceed by scanning the parameters $K_{\rm sat} = \mathcal{O}(1)$, $\beta \in [0, 1]$ and $\eta/s(T)$. In particular, we vary the minimum value and slopes of $\eta/s(T)$, keeping its general shape as in Fig. 2. Both the BJ and FS prethermal evolutions are considered. In practice, for each fixed $\{\beta, {\rm BJ/FS}, \eta/s(T)\}$, the remaining parameter $K_{\rm sat}$ is always tuned such that the multiplicity in the 0–5% most central collisions at the LHC is reproduced.

In Fig. 3a we show the computed centrality dependence of the charged hadron multiplicity in Pb+Pb collisions at $\sqrt{s_{NN}} = 2.76$ TeV compared with the ALICE data [41]. As demonstrated here, several sets $\{K_{\rm sat}, \beta, {\rm BJ/FS}, \eta/s(T)\}$ give a good agreement with the measurement. However, the data clearly favors $\beta \sim 1$ and slightly the FS scenario over the BJ. For comparison, we also show the results obtained with the usual (non-saturation) eBC and eWN Glauber model initial states [42].

In Fig. 3b we show the multiplicities for Au+Au collisions at $\sqrt{s_{NN}} = 200$ GeV, using the same parameter sets $\{K_{\rm sat}, \beta, {\rm BJ/FS}, \eta/s(T)\}$ as in panel 3a, and compare with the PHENIX [43] and STAR [26] data. We note that although the RHIC data would seem to favor a slightly smaller β and the BJ case, the overall simultaneous agreement at RHIC and LHC is rather good.

As long as the centrality dependence of the multiplicity is described, all the scenarios studied here give a very good description of the charged hadron $p_{\rm T}$-spectra. More relevant parameters in this case are $T_{\rm chem}$ and $T_{\rm dec}$ which here are kept unchanged from RHIC to LHC. The obtained p_T spectra are shown in Fig. 3c for the LHC and in Fig. 3d for RHIC. The data are from Refs. [44] and Ref. [45,46], correspondingly.

In Figs. 3e and 3f we show the elliptic flow coefficients $v_2(p_{\rm T})$ at the LHC and RHIC, respectively. The data are from ALICE [47] and STAR [48]. The $v_2(p_{\rm T})$ coefficients depend strongly on the η/s parametrization, and, e.g., an ideal fluid description (not shown) does not give a correct $v_2(p_{\rm T})$. By scanning the $\eta/s(T)$ as explained above, while keeping $K_{\rm sat}$ of order 1, we observed that a good simultaneous agreement with the measurements is obtained with the cases shown in Fig. 2. We emphasize that at RHIC, where the flow gradients are larger at decoupling, one should require the agreement in particular in the small-p_T region, where the dissipative corrections to the particle distributions do not grow unphysically large. Note especially that since $\eta/s(T)$ is considered as a material property, it must not be changed between different collision systems.

First, we note that the rather weak temperature dependence of QGP η/s in the $\eta/s(H)$ parametrization does not affect the elliptic flow significantly compared to the $\eta/s(L)$ parametrization, but rather reflects into the entropy production that has to be compensated by changing $K_{\rm sat}$. A higher collision energy is required to get an access to the high temperature behavior of η/s [11,12]. The most important parts of the $\eta/s(T)$ parametrization that affect $v_2(p_T)$ are its minimum value and the slope of the hadronic $\eta/s(T)$. The data sets used here do not uniquely fix these parameters, but the change in the minimum value can be compensated by changing the hadronic slope, e.g., an equally good simultaneous fit can be obtained by a constant $\eta/s \sim 0.20$, which is similar in magnitude as obtained in Refs. [2–10]. However, a more realistic hadronic η/s should increase with decreasing temperature, see Ref. [49]. Imposing this behavior, and requiring a fit to the data, the η/s minimum will be below such an overall constant value. In the linear parametrizations shown in Fig. 2 $\eta/s_{\rm min} = 0.12$ at $T = 180$ MeV, and $\eta/s = 0.32$ (0.30) at $T = 100$ (500) MeV. Steeper slopes in the hadronic η/s (as in Refs. [11,12]) than used here would lead to underpredicting $v_2(p_T)$ even at smaller p_T than in Fig. 3f.

It is important to keep in mind, as discussed in Refs. [3,6–8,11], that the conclusions of the allowed η/s ranges are sensitive to the initial conditions and coefficients of the higher-order dissipative terms in the fluid-dynamical equations: in Ref. [5] which also uses QCD-based computed initial conditions, a qualitatively similar fit to the LHC and RHIC $v_2(p_T)$ was obtained with the η/s parametrizations of Refs. [11,12] as we do here with the parametrizations in Fig. 2. With this, we underline the importance of understanding the QCD matter initial conditions as well as a multiobservable analysis such as presented here.

To conclude, we computed the energy density profiles and formation times of the produced QGP at the LHC and RHIC in a new NLO-improved pQCD + local saturation model of considerable predictive power. The subsequent evolution of these initial conditions was described with dissipative fluid dynamics. Identifying the model uncertainties, a good global agreement with the measured centrality dependence of the low-p_T bulk observables

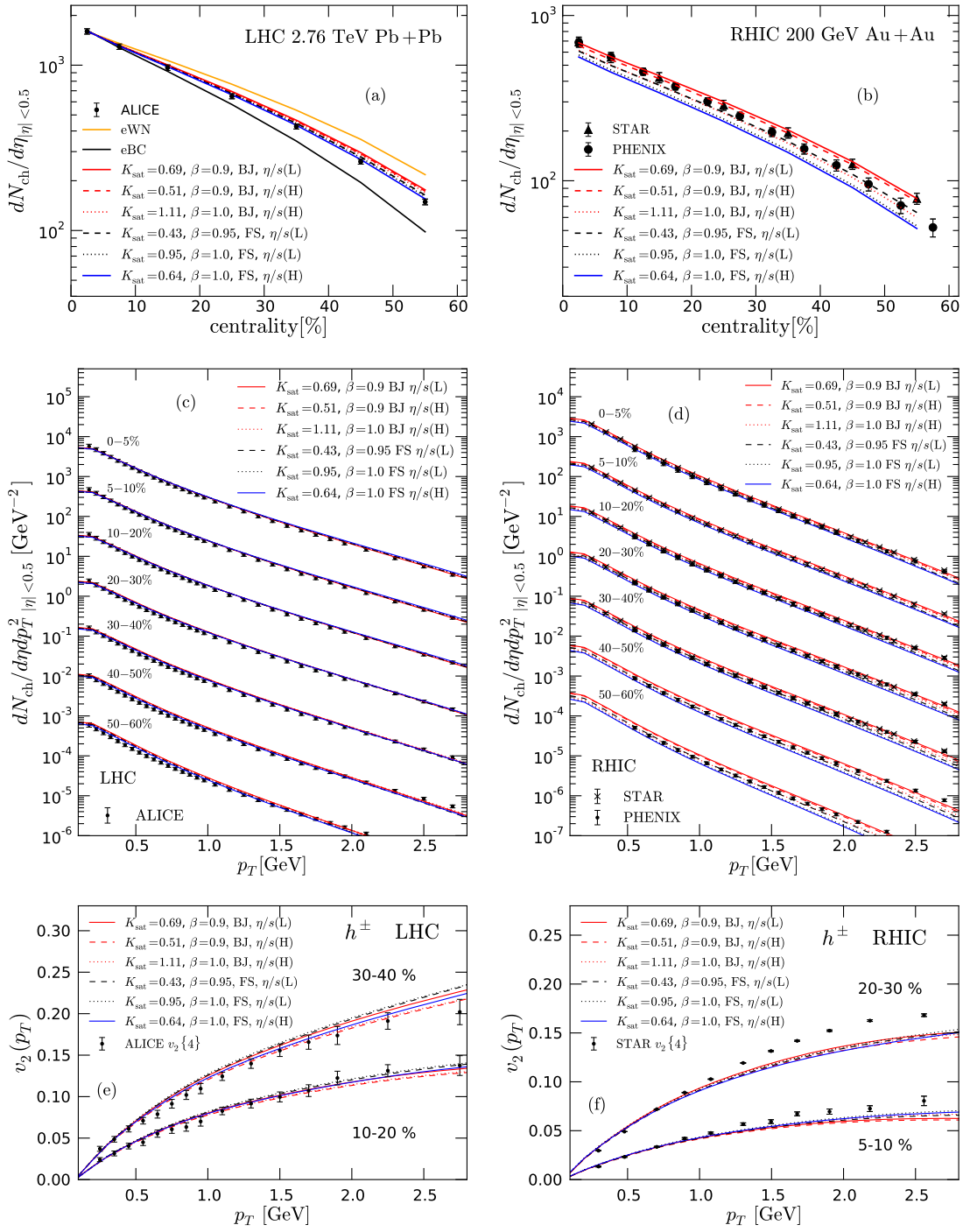

Fig. 3. (Color online.) Centrality dependence of the charged hadron multiplicity at the LHC (a) and RHIC (b). Transverse momentum spectra of charged hadrons at the LHC (c) and RHIC (d), in the same centrality classes as the ALICE data in panel (a), and scaled down by increasing powers of 10. Elliptic flow coefficients $v_2(p_T)$ at the LHC (e) and RHIC (f), compared with the measured 4-particle cumulant $v_2\{4\}(p_T)$. Labeling of the theory curves in each panel is identical, and the parameter sets $\{K_{sat}, \beta, \text{BJ/FS}, \eta/s(T)\}$ are indicated. The labels H and L refer to Fig. 2.

was obtained simultaneously at the LHC and RHIC. In particular, we were able to constrain the $\eta/s(T)$ parametrization simultaneously by all these data. In the future, we will extend this analysis to include event-by-event fluctuations.

Acknowledgements

This work was financially supported by the Wihuri Foundation (R.P.) and the Academy of Finland, projects 133005 (K.J.E.) and 267842 (K.T.). We thank I. Helenius, T. Lappi, H. Mäntysaari and H. Paukkunen for useful discussions, and CSC-IT Center Science for supercomputing time.

References

[1] For a recent review and references, see U.W. Heinz, R. Snellings, Annu. Rev. Nucl. Part. Sci. 63 (2013) 123.
[2] P. Romatschke, U. Romatschke, Phys. Rev. Lett. 99 (2007) 172301.
[3] M. Luzum, P. Romatschke, Phys. Rev. C 78 (2008) 034915;

M. Luzum, P. Romatschke, Phys. Rev. C 79 (2009) 039903 (Erratum).
[4] B. Schenke, S. Jeon, C. Gale, Phys. Rev. Lett. 106 (2011) 042301;
B. Schenke, S. Jeon, C. Gale, Phys. Rev. C 85 (2012) 024901;
B. Schenke, S. Jeon, C. Gale, Phys. Lett. B 702 (2011) 59.
[5] C. Gale, et al., Phys. Rev. Lett. 110 (2013) 012302.
[6] H. Song, et al., Phys. Rev. Lett. 106 (2011) 192301;
H. Song, et al., Phys. Rev. Lett. 109 (2012) 139904 (Erratum);
H. Song, et al., Phys. Rev. C 83 (2011) 054910;
H. Song, et al., Phys. Rev. C 86 (2012) 059903 (Erratum).
[7] H. Song, S.A. Bass, U. Heinz, Phys. Rev. C 83 (2011) 054912;
H. Song, S.A. Bass, U. Heinz, Phys. Rev. C 87 (2013) 019902 (Erratum).
[8] C. Shen, U. Heinz, P. Huovinen, H. Song, Phys. Rev. C 82 (2010) 054904;
C. Shen, U. Heinz, P. Huovinen, H. Song, Phys. Rev. C 84 (2011) 044903.
[9] P. Bozek, Phys. Rev. C 81 (2010) 034909;
P. Bozek, Phys. Rev. C 85 (2012) 034901.
[10] P. Bozek, I. Wyskiel-Piekarska, Phys. Rev. C 85 (2012) 064915.
[11] H. Niemi, et al., Phys. Rev. C 86 (2012) 014909.
[12] H. Niemi, et al., Phys. Rev. Lett. 106 (2011) 212302.
[13] L.V. Gribov, E.M. Levin, M.G. Ryskin, Phys. Rep. 100 (1983) 1.
[14] A.H. Mueller, J. Qiu, Nucl. Phys. B 268 (1986) 427.
[15] L.D. McLerran, R. Venugopalan, Phys. Rev. D 49 (1994) 2233.
[16] K.J. Eskola, K. Kajantie, Z. Phys. C 75 (1997) 515.
[17] K.J. Eskola, K. Kajantie, P.V. Ruuskanen, K. Tuominen, Nucl. Phys. B 570 (2000) 379.
[18] R. Paatelainen, K.J. Eskola, H. Holopainen, K. Tuominen, Phys. Rev. C 87 (2013) 044904.
[19] K.J. Eskola, H. Paukkunen, C.A. Salgado, J. High Energy Phys. 0904 (2009) 065.
[20] F. Gelis, E. Iancu, J. Jalilian-Marian, R. Venugopalan, Annu. Rev. Nucl. Part. Sci. 60 (2010) 463.
[21] K.J. Eskola, P.V. Ruuskanen, S.S. Räsänen, K. Tuominen, Nucl. Phys. A 696 (2001) 715.
[22] K.J. Eskola, H. Niemi, P.V. Ruuskanen, S.S. Räsänen, Phys. Lett. B 566 (2003) 187.
[23] K.J. Eskola, et al., Phys. Rev. C 72 (2005) 044904.
[24] T. Renk, H. Holopainen, R. Paatelainen, K.J. Eskola, Phys. Rev. C 84 (2011) 014906.
[25] K.J. Eskola, K. Kajantie, K. Tuominen, Phys. Lett. B 497 (2001) 39.
[26] B.I. Abelev, et al., STAR Collaboration, Phys. Rev. C 79 (2009) 034909.
[27] K.J. Eskola, K. Kajantie, J. Lindfors, Nucl. Phys. B 323 (1989) 37.
[28] K.J. Eskola, K. Tuominen, Phys. Lett. B 489 (2000) 329;
K.J. Eskola, K. Tuominen, Phys. Rev. D 63 (2001) 114006.
[29] J. Pumplin, et al., J. High Energy Phys. 0207 (2002) 012.
[30] I. Helenius, K.J. Eskola, H. Honkanen, C.A. Salgado, J. High Energy Phys. 1207 (2012) 073.
[31] Z. Kunszt, D.E. Soper, Phys. Rev. D 46 (1992) 192.
[32] K.J. Eskola, K. Kajantie, K. Tuominen, Nucl. Phys. A 700 (2002) 509.
[33] H. Niemi, G.S. Denicol, H. Holopainen, P. Huovinen, Phys. Rev. C 87 (2013) 054901.
[34] W. Israel, J.M. Stewart, Proc. R. Soc. A 365 (1979) 43;
W. Israel, J.M. Stewart, Ann. Phys. 118 (1979) 341.
[35] G.S. Denicol, H. Niemi, E. Molnar, D.H. Rischke, Phys. Rev. D 85 (2012) 114047.
[36] E. Molnar, H. Niemi, G.S. Denicol, D.H. Rischke, arXiv:1308.0785 [nucl-th].
[37] E. Molnar, H. Niemi, D.H. Rischke, Eur. Phys. J. C 65 (2010) 615.
[38] F. Cooper, G. Frye, Phys. Rev. D 10 (1974) 186.
[39] P. Huovinen, P. Petreczky, Nucl. Phys. A 837 (2010) 26.
[40] L.P. Csernai, J.I. Kapusta, L.D. McLerran, Phys. Rev. Lett. 97 (2006) 152303.
[41] K. Aamodt, et al., ALICE Collaboration, Phys. Rev. Lett. 106 (2011) 032301.
[42] P.F. Kolb, et al., Nucl. Phys. A 696 (2001) 197.
[43] S.S. Adler, et al., PHENIX Collaboration, Phys. Rev. C 71 (2005) 034908;
S.S. Adler, et al., Phys. Rev. C 71 (2005) 049901 (Erratum).
[44] B. Abelev, et al., ALICE Collaboration, Phys. Lett. B 720 (2013) 52.
[45] J. Adams, et al., STAR Collaboration, Phys. Rev. Lett. 91 (2003) 172302.
[46] S.S. Adler, et al., PHENIX Collaboration, Phys. Rev. C 69 (2004) 034910.
[47] K. Aamodt, et al., ALICE Collaboration, Phys. Rev. Lett. 105 (2010) 252302.
[48] Y. Bai, PhD thesis, Nikhef and Utrecht University, The Netherlands, 2007;
A. Tang, STAR Collaboration, arXiv:0808.2144 [nucl-ex].
[49] J. Noronha-Hostler, J. Noronha, C. Greiner, Phys. Rev. Lett. 103 (2009) 172302.